Switchable dynamic Rydberg-dressed excitation via a cascaded double electromagnetically induced transparency

Yichun Gao, Yinghui Ren, Dongmin Yu, and Jing Qian*

State Key Laboratory of Precision Spectroscopy, Quantum Institute for Light and Atoms, Department of Physics, School of Physics and Electronic Science, East China Normal University, Shanghai 200062, China

(Received 12 May 2019; published 17 September 2019)

Dynamic control of atomic dressing to the highly excited Rydberg state in multilevel systems has special appeals owing to the development of flexible and precise measurement. In this study we develop an experimentally accessible proposal to robustly control the dressing probability via a three-step cascaded excitation with double electromagnetically induced transparency (EIT) technique. The system can function as an optical switch where the third addressing laser serving as the control knob can switchably engineer the dressing probability with time. Differing from a conventional two-photon EIT, this scheme facilitates a maximal dressing probability determined by a relative strength between two strong coupling fields, entirely relaxing their absolute values. The collective feature caused by the interactions of a few atoms is also studied leading to an enhanced dressing probability as well as reduced response times. Our work offers the opportunity to a coherent dynamic control of Rydberg excitation and to realize sizable Rydberg-Rydberg interactions in weakly driven multilevel quantum systems.

DOI: 10.1103/PhysRevA.100.033823

I. INTRODUCTION

Rydberg-dressed atoms working in a regime with only a small fraction of excited atoms, promises the sizable long-range interaction to megahertz as well as the enhanced lifetime up to a few seconds [1,2]. They have great prospectives for studies in the fields of strongly correlated many-body physics [3–6], the laser-driven quantum magnetism [7,8] and the micro-devices for quantum information processing [9–11]. The route to Rydberg dressing can be accessible via Rydberg electromagnetically induced transparency (Rydberg-EIT) [12–14] which can stimulate resonant optical driving by the establishment of a dark state weakly dressed to a Rydberg level [15], opening up new research avenues for nonlinear quantum optics [16].

The optical control of resonant dipole-dipole interactions has been realized in a four-level protocol with two upper Rydberg levels coupled by a microwave field, inducing exchange interaction between them [17]. Such a multistep scheme to highly excited Rydberg states is sufficiently appealing because it enables a Rydberg state to be easily reached by nearby-level transitions with inexpensive lasers [18,19]. Besides, it experimentally benefits from a kick-free and Doppler-free excitation that can produce a narrow resonance linewidth. So far, a few pioneer works studying EIT effect in a four-level atomic system originated from Agarwal [20] and Harris [21], which describe the absorption of two photons controlled by quantum interference between two excitation paths. Later, a number of theoretical works on the nonlinear optical feature are represented in similar systems [22–24]. Recently a more complex four-step excitation scheme is achieved in which the uppermost Rydberg state has a larger dipole moment [25].

However, most studies have been limited to the steady-state property of the probe field, revealing stable transmission signals in, e.g., hollow-core fibers [26]; yet a coherent dynamic control for the atomic dressing to a Rydberg level is still rarely reported, mainly because of the complexity of using multiple lasers in multilevel systems. Recently Zhang *et al.* studied the transient probe absorption response of a Rydberg-EIT via a sudden switch-on of the coupling field, bringing one-step closer to this target [27]; nevertheless, a systematic study of the dynamic control and response property remains elusive.

In the present work, we propose a study of the practical dynamic dressing process to a target Rydberg level via a three-photon excitation in a four-level cascaded system. A usual two-step EIT can couple a ground state to a long-lived nS or nD state by the transition rules [28–31]. Here, the uppermost state is nP-type, which has to use at least a three-step excitation where the third time-dependent addressing field serving as a control knob, will result in a split for the probe field transparency window, referred to as a double Rydberg-EIT [32]. In spite of the complexity of system, the advantage of using a four-level configuration lies in existing a maximal dressing probability that is only determined by the relative strength between two strong coupling lasers, rather than their absolute values. That means, with an auxiliary middle field an analytical constraint condition is derived that quantitatively describes the required relationship among three lasers, for the realization of a maximal dressing probability in a four-level cascaded system.

In addition, we also study the transient dynamics and time responses of the system, presenting the role of Rydberg blockaded interaction in the reduction of response time, accompanied by an enhanced probability due to the collective feature on dark-state resonance of interacting atoms [33]. That effect is improved with the number of atoms. Note that in Ref. [27] authors focus on the transient optical responses of

*Corresponding author: jqian1982@gmail.com

the probe absorption in a three-level Rydberg-EIT, not of the dynamic dressing excitation. The typical response time for probe absorption is shorter, especially for the fall time. An experimental proposal is discussed by switching on or off the addressing field under flexible parameters, powerfully proving the realization of a robust atomic dressing excitation with savable laser powers in a real implementation. Our results provide an easy treatment to develop the process of multilevel Rydberg dressing with optimal dressing probability and response time, facilitating its extensive uses in developing all-optical switches and transistor devices [34–37].

II. THEORETICAL MODEL AND STEADY STATE

A. Double-electromagnetically induced transparency

Since the generalized EIT based on N-level cascaded schemes was analyzed in Ref. [38], it may be helpful to recall the essence of a specific double-EIT based on a cascade-configuration where the upper states are twofold. The scheme consists of a three-photon cascaded excitation to a Rydberg state $|r\rangle$ following $|g\rangle \to |m\rangle \to |e\rangle \to |r\rangle$, performed by one weak probe laser Ω_p, one strong coupling laser Ω_1 and one addressing coupling laser $\Omega_2(t)$ with amplitude Ω_{20} [see Fig. 1(a)]. In the frame rotating with the frequencies of laser fields, the atom-field interaction Hamiltonian $\mathcal{H}_1$ reads ($\hbar = 1$)

$$\hat{\mathcal{H}}_1 = \hat{\mathcal{H}}_{1,0} + \frac{1}{2}(\Omega_p \hat{\sigma}_{1,gm} + \Omega_1 \hat{\sigma}_{1,me} + \Omega_{20}\hat{\sigma}_{1,er} + \text{H.c.}), \tag{1}$$

where $\hat{\mathcal{H}}_{N,0} = -[\Delta_m \hat{\sigma}_{1,mm} + (\Delta_m + \Delta_e)\hat{\sigma}_{1,ee} + (\Delta_m + \Delta_e + \Delta_r)\hat{\sigma}_{1,rr}]$ describes the atomic self-energy under resonance: $\Delta_e = \Delta_r = 0$ and $\hat{\sigma}_{1,\alpha\beta} = |\alpha\rangle_1\langle\beta|$ is the projection operator. The subscript "1" means one-atom case. In experiment detuning Δ_m can be easily adjusted by the probe laser frequency for observing the transmission signals of probe field.

In the dressed-state scenario, for the two stronger coupling fields, i.e., $\Omega_1, \Omega_{20} \gg \Omega_p$ (we define $\Omega_{\text{eff}} = \sqrt{\Omega_1^2 + \Omega_{20}^2}$), the eigenvalues in the subspace with $\{|m\rangle, |e\rangle, |r\rangle\}$ are $E_{\Phi_0} = -\Delta_m$, $E_{\Phi_\pm} = \frac{1}{2}(-2\Delta_m \pm \Omega_{\text{eff}})$ and the corresponding bright eigenstates are given by

$$|\Phi_0\rangle = \frac{1}{\Omega_{\text{eff}}}(-\Omega_{20}|m\rangle + \Omega_1|r\rangle), \tag{2}$$

$$|\Phi_\pm\rangle = \frac{1}{\sqrt{2}\Omega_{\text{eff}}}(\Omega_1|m\rangle \pm \Omega_{\text{eff}}|e\rangle + \Omega_{20}|r\rangle). \tag{3}$$

In the limit of $\Omega_{20} \to 0$ the scheme works as a conventional EIT between $|g\rangle$ and $|e\rangle$ where the quantum interference in the absorption of probe transmission leads to a single dark resonance in the center, see the dashed curve in Fig. 1(b). The third dressed state $|\Phi_0\rangle$ in this limit related to $|r\rangle$ only, is decoupled from the system, entirely suppressing the excitation of $|r\rangle$ then. With the presence of Ω_{20}, the zero-energy dark state $|g\rangle$ will be coupled to three bright eigenstates by resonant excitations through the pathways of $|g\rangle \to |\Phi_{0,\pm}\rangle$ at $\Delta_m = 0, \pm\frac{\Omega_{\text{eff}}}{2}$ respectively, as presented in the inset of Fig. 1(b), producing double dark states at $\Delta_m = \pm\Omega_{20}/2$ via the quantum interference among them. As a consequence, the system becomes transparent to a weak probe field in two EIT windows based on double dark states, which leads to an

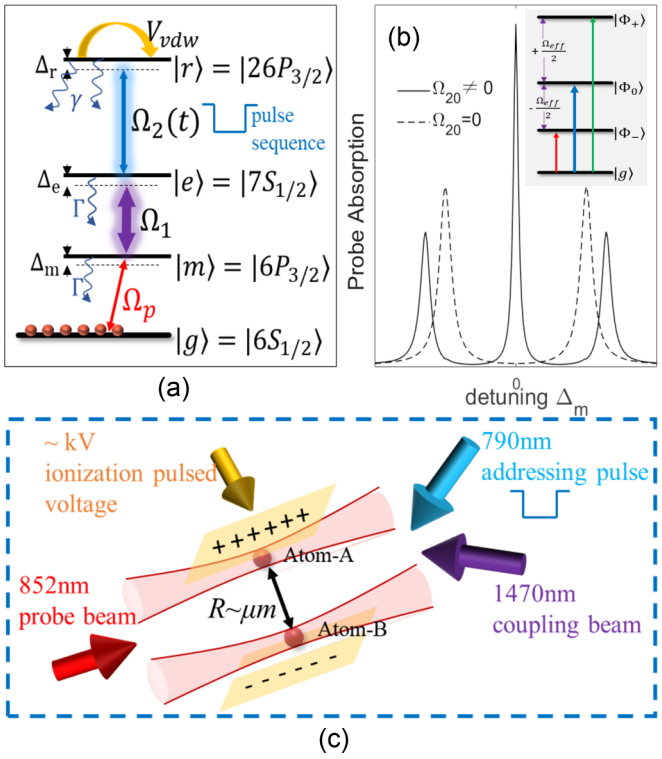

FIG. 1. Schematics of a controlled three-step Rydberg dressing excitation. (a) Energy levels and the atom-field interactions. Ground-state atoms are dressed to a Rydberg state $|r\rangle$ via a cascaded process $|g\rangle \to |m\rangle \to |e\rangle \to |r\rangle$. Real energy levels are shown based on ^{133}Cs atoms. (b) Probe absorption (arbitrary unit) versus detuning Δ_m in the cases of $\Omega_{20} = 0$ and $\Omega_{20} \neq 0$. The inset shows the dressing excitation through pathways of $|g\rangle \to |\Phi_{0,\pm}\rangle$. (c) The experimental setup (proposal). Two Cs atoms are trapped in tightly focused dipole traps with the interstate spacing $R \sim \mu m$, detected by using a pulse field ionization with a high voltage $\sim kV$. The required laser beams are also shown.

improved absorption peak occurring in the center $\Delta_m = 0$, aside from two Autler-Townes peaks at $\Delta_m = \pm\frac{\Omega_{\text{eff}}}{2}$ [see the solid curve in Fig. 1(b)]. This phenomenon of interfering double dark states can be described by a double-EIT scenario where the improved probe absorption in the center is caused by the coherent interaction between two distinct dark resonances [39].

In the present work, we propose that the addressing laser $\Omega_2(t)$ with amplitude Ω_{20} is a square-wave pulse sequence, acting as a control knob to the dynamic excitation of Rydberg-dressed state. An experimental setup represented in Fig. 1(c) contains three optical fields with wavelengths 852 nm, 1470 nm, and 790 nm, corresponding to the transitions of $|g\rangle \to |m\rangle$, $|m\rangle \to |e\rangle$ and $|e\rangle \to |r\rangle$, respectively. The additional measurement can be performed by using an ultra-short high-voltage electric pulse for ionization of Rydberg state atoms, accompanied by a time of flight spectra detecting ions or electrons [40].

B. Steady probe absorption

First we investigate the steady probe absorption of the double Rydberg-EIT which can be obtained by solving the

master equation:

$$\frac{d\hat{\rho}}{dt} = i[\hat{\rho}, \hat{\mathcal{H}}_1] + \hat{\mathcal{L}}_1(\hat{\rho}), \tag{4}$$

where the Lindblad operator taking into account dissipation can be demonstrated as

$$\hat{\mathcal{L}}_1(\hat{\rho}) = \Gamma \sum_{\alpha\beta}[\hat{\sigma}_{1,\alpha\beta}\hat{\rho}\hat{\sigma}_{1,\beta\alpha} - \frac{1}{2}(\hat{\sigma}_{1,\beta\beta}\hat{\rho} + \hat{\rho}\hat{\sigma}_{1,\beta\beta})]$$
$$+ \gamma \sum_{ij}[\hat{\sigma}_{1,ij}\hat{\rho}\hat{\sigma}_{1,ji} - \frac{1}{2}(\hat{\sigma}_{1,jj}\hat{\rho} + \hat{\rho}\hat{\sigma}_{1,jj})], \tag{5}$$

with $\alpha\beta \in \{gm, me\}$, $ij \in \{er, gr\}$. Γ and γ are the spontaneous decay rates of middle excited $|m(e)\rangle$ and Rydberg levels $|r\rangle$, typically $\gamma/\Gamma \approx 0.01$.

In the weak probe limit where all population is assumed to be in the ground state by letting $\rho^s_{gg} = 1$ (others $\rho^s_{mm} = \rho^s_{ee} = \rho^s_{rr} = 0$ and the superscript s means the steady state), the nondiagonal steady element ρ^s_{gm} demonstrating the coherence of probe transition, can be expressed as

$$\rho^s_{gm} = i\Omega_p \frac{\Omega_{20}^2 + X_1X_2}{X_1\Omega_{20}^2 + X_2\Omega_1^2 + X_1^2X_2}, \tag{6}$$

with $X_1 = \Gamma + 2i\Delta_m$, $X_2 = 2\gamma + 2i\Delta_m$ and $\Gamma_m = \Gamma_e = \Gamma$, $\Gamma_r = \gamma$. The steady-state solutions ρ^s_{ij}, defined by

$$\rho^s_{ij} = \rho_{ij}(t \to \infty) \tag{7}$$

can be analytically derived by considering $\dot{\rho}_{ij} = 0$, coinciding with the results from numerically solving Eq. (4). In the simulation the typical time for the states to be stationary is, e.g., $t > 100/\Gamma$ with $\Gamma(\Gamma^{-1})$ used as the frequency(time) unit throughout the paper. Here the steady probe absorption $(\rho^s_{gm})^I$ can be derived from the imaginary part of ρ^s_{gm}, as well as the steady dressing probability ρ^s_{rr} to the first-order approximation takes a more complex form, as described in Eqs. (A2)–(A5) of Appendix A.

For an intuitive understanding, relevant eigenvalues with respect to Δ_m are comparably plotted in Fig. 2(a). It is clear that the zero-energy dark state $|g\rangle$ avoidably crossed by three bright eigenvalues E_{Φ_0} and $E_{\Phi_\pm}$ at $\Delta_m = 0, \pm\Omega_{\text{eff}}/2$, arise enhanced probe absorption there, see Fig. 2(b). However, $|\Phi_\pm\rangle$ is unsuited for atomic dressing to Rydberg state due to its nonnegligible occupancy on middle state $|e\rangle$, i.e., $\rho^s_{ee} \equiv \frac{1}{2}$; whereas if $(\Omega_{20}/\Omega_{\text{eff}})^2 \ll 1$, $|\Phi_0\rangle \approx (\Omega_1/\Omega_{\text{eff}})|r\rangle$ is a good candidate for the dressing based on its resonance with $|g\rangle$ at $\Delta_m = 0$ as well as its complete immunity to the middle excited states.

The steady peak probe absorption $(\rho^I_{gm})^s$ at $\Delta_m = 0, \pm\Omega_{\text{eff}}/2$ are represented in Fig. 2(c), versus the increase of Ω_{20}. As expected, for a conventional EIT with $\Omega_{20} = 0$ the probe laser experiences no absorption in the center arising zero excitation probability there. By increasing Ω_{20} the central resonant absorption induced by constructive quantum interference between double dark states at $\Delta_m = \pm\Omega_{20}/2$, obtains a substantial growth accompanied by a slight reduction for the sideband absorptions at $\Delta_m = \pm\Omega_{\text{eff}}/2$.

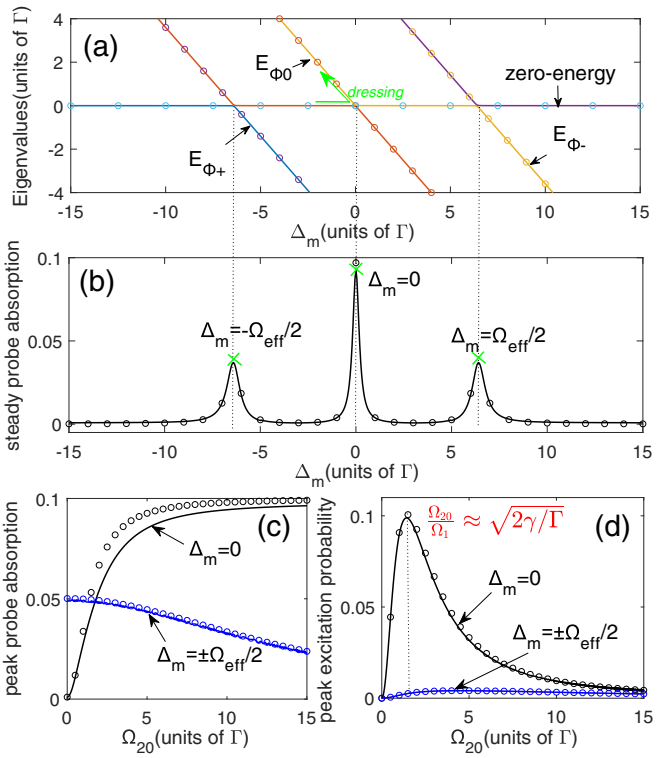

FIG. 2. (a) The eigenvalues and (b) the steady probe absorption $(\rho^I_{gm})^s$, versus the detuning Δ_m. Three absorption peaks emerge at the avoided crossings $\Delta_m = 0, \pm\Omega_{\text{eff}}/2$. Relevant parameters used are $(\Omega_1, \Omega_p, \Omega_{20}) = (10, 0.1, 8)$, $\gamma = 0.01$ and Γ is the frequency unit. The peak strength of probe absorption in (c) and the peak dressing probability in (d) at $\Delta_m = 0$ (black) and $\pm\Omega_{\text{eff}}/2$ (blue) versus the strength of the addressing laser. The rendered numerical results(solid) are consistent with the analytical plot (circles) of the derived stationary formulas.

C. Maximal steady Rydberg dressing

Figure 2(d) shows the peak dressing probability ρ^s_{rr} as a function of Ω_{20}. For improving ρ^s_{rr} it requires a direct connection between $|g\rangle$ and $|\Phi_0\rangle$ at the avoided crossing, as shown by a green arrow in Fig. 2(a). From Eq. (2), we see that the steady occupancy in $|m\rangle$ must be minimized under $\rho^s_{mm} \propto (\Omega_{20}/\Omega_1)^2 \ll 1$, agreeing with the finding in Fig. 2(d) that the optimal (maximal) value occurs at $\Omega_{20}/\Omega_1 \approx 0.14$ (quite small). In fact, via a differential calculation to the Eq. (A4) we are able to obtain a generalized constraint condition $\Omega_{20}/\Omega_1 \approx \sqrt{2\gamma/\Gamma}$, by which the maximal value is $(\rho^s_{rr})^{\max} = \frac{(1+2\gamma)\Omega_p^2}{2\Omega_p^2+4\gamma(2+\gamma)} \approx 0.10$, coinciding with numerical results. In other words, it is possible to maximize the dressing probability in a four-level configuration, by optimizing the relative strength between two coupling Rabi frequencies Ω_1 and Ω_{20} rather than their absolute values, which provides a more flexible selection of lasers in the implementation. Additionally, note that if Ω_{20} is even larger, for $\Delta_m = 0$ the steady population ρ^s_{rr} has a quick decrease owing to the effect of $|m\rangle$ while at off-resonance it keeps a low value due to its poor dressing probability with other bright states $|\Phi_\pm\rangle$.

To this end we will focus on the case of $\Delta_m = 0$ in the following.

III. DYNAMIC ATOMIC DRESSING TO RYDBERG STATES

In experiment, a study of transient behavior for dynamic dressing to a Rydberg state is significantly important, requiring a sensitive measurement. Here we theoretically investigate the dynamic dressing excitation of one-atom system where the addressing laser is replaced by a time-dependent pulse $\Omega_2(t)$, simulating "switch-OFF" and "switch-ON" cases with respect to $\Omega_2(t) = 0$ and $\Omega_2(t) = \Omega_{20}$. Intuitively, when $\Omega_2(t)$ is turned off, it completely closes the excitation and if $\Omega_2(t)$ is turned to be ON, the dressing dynamics experiencing a fast response speed ($\sim\mu s$), arrives at a new higher steady state. Numerical results for the transient dynamics and fast responses are obtained by directly solving the optical Bloch equations [see Eqs. (A1) in Appendix A] where the dephasing effects acting on coherence due to transit time broadening and laser intensity variations are ignored.

The performance of such an optical switch can be quantified by two important parameters: transient excitation probability $P_{1,r}(t)$ and transient response time $\tau_{1,r(d)}$,

(i) $P_{1,r}(t)$ denotes the time-dependent Rydberg dressing probability with $P_{1,r}^{\rm on}$ and $P_{1,r}^{\rm off}[\equiv 0]$ standing for the values of transient dressing probabilities when $\Omega_2 = \Omega_{20}$ and $\Omega_2 = 0$ are applied. Strongly differing from a conventional two-photon EIT, here the auxiliary middle laser Ω_1 offers an optimal adjustment to maximize the excitation probability of the dressed state.

(ii) $\tau_{1,r(d)}$ represents the transient response time, i.e., the least required time for attaining a new steady state after a sudden switch of the pulse $\Omega_2(t)$. $\tau_{1,r}$ and $\tau_{1,d}$, respectively, point to the rise time and fall time, see the inset of Fig. 3(b).

As represented in Fig. 2(d) the steady dressing probability ρ_{rr}^s has a significant growth at $\Delta_m = 0$, agreeing with the results of Fig. 3(a1) where we show the transient dressing probability $P_{1,r}^{\rm on}$ versus Δ_m and Ω_{20}, and an obvious enhancement on resonance is verified. An enlarged view in the inset reveals a similar behavior as Fig. 2(d)(black solid) that $P_{1,r}^{\rm on}$ continuously decreases after its peak value at $\Omega_{20}/\Omega_1 \approx \sqrt{2\gamma/\Gamma}$, strongly proving the importance of a suitable ratio Ω_{20}/Ω_1 for maximizing the dressing probability. The correctness of this argument can also be certified in Fig. 3(a2) where we globally study the dependence of $P_{1,r}^{\rm on}$ on relative Rabi frequencies Ω_1/Ω_p and Ω_{20}/Ω_1. It is remarkably noting that the transient dressing probability can robustly sustain it maximal value $\approx$0.10 only when two conditions of

$$\Omega_{20}/\Omega_1 \approx \sqrt{2\gamma/\Gamma}, \quad \Omega_1/\Omega_p \gg 1 \tag{8}$$

are simultaneously met. Here $\Omega_1/\Omega_p \geqslant 50$ obtained numerically is the least requirement and this value will slightly change by Ω_p. In other words, the absolute values of optical Rabi frequencies are fully irrelevant in our scheme as long as Eq. (8) is preserved, providing a more flexible way to realize an improving Rydberg probability of dressed state with much reduced laser powers [see Sec. V for a detailed discussion].

For gaining a deep and complete insight, we further study the second parameter $\tau_{1,r(d)}$ by dynamically switching $\Omega_2(t)$ [see the inset of Fig. 3(b)], and record the required response times for a new steady state after the sudden switches. Figure 3(b) represents the fall time $\tau_{1,d}$ and the rise time $\tau_{1,r}$ as a function of Ω_{20}/Ω_1 for different Ω_1 values. Note that

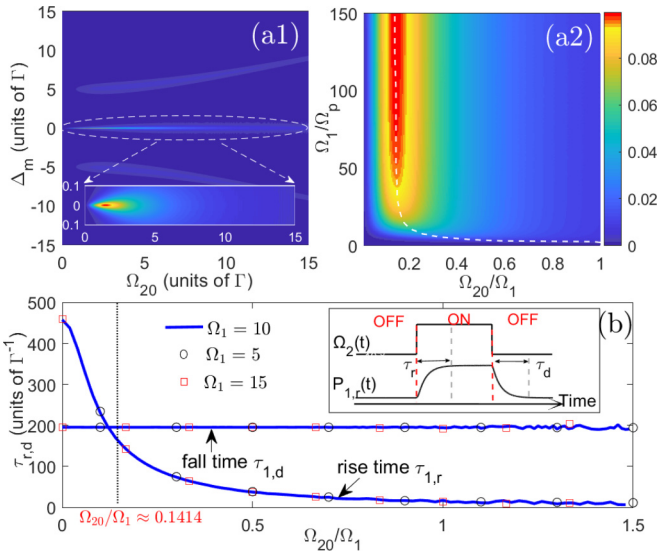

FIG. 3. In switch-ON case, the transient excitation probability $P_{1,r}^{\rm on}$ versus the variations of amplitudes Ω_{20} and Δ_m in (a1), as well as of the ratios Ω_{20}/Ω_1 and Ω_1/Ω_p in (a2). Inset of (a1) is an enlarged picture for $\Delta_m \in [-0.1, 0.1]$. In (a2) the local maximal values with respect to a given ratio Ω_1/Ω_p are denoted by a white-dashed curve. (b) The transient response time $\tau_{1,r(d)}$ (rise time and fall time), versus the change of ratio Ω_{20}/Ω_1 for $\Omega_1 = 10$ (blue solid), 5 (black circles), 15 (red squares). It keeps $\Omega_p = 0.1$. Inset of (b) shows a complete one-period dynamics of Rydberg dressing probability $P_{1,r}(t)$ under the control pulse $\Omega_2(t)$. Here $\gamma = 0.01$ and Γ is treated as the frequency unit in the calculation.

the condition $\Omega_1/\Omega_p \gg 1$ is preserved. Surprisingly, the fall time $\tau_{1,d}$ is observed to be a constant irrespective of the laser drivings because when $\Omega_2(t)$ is switched off, the system always tends toward a same final state with $P_{1,r}^{\rm off} \equiv 0$, arising $\tau_{1,d}$ decided by the decay rate γ only (see Table I for a detailed comparison of different decay rates). If one reduces γ by exciting to a higher-n Rydberg state, then it needs more time to be stable. In contrast, the rise time $\tau_{1,r}$ exhibits a rapid decrease with the increase of Ω_{20}/Ω_1, essentially caused by a stronger excitation between $|e\rangle$ and $|r\rangle$ with a larger Ω_{20} or a smaller Ω_1, reducing the time to be stationary. Also it needs to stress again that only the relative strengths of optical Rabi frequencies not their absolute strengths play roles, because different Ω_1 values give rise to exactly same response times in our proposal.

In Appendix B we give more information for comparing the response times between the steady probe absorption and the dressing excitation dynamics. To our knowledge, a sudden switch of the addressing field $\Omega_2(t)$ can cause a transient optical response for the probe field absorption, subsequently arising a tendency toward a new steady dressing state within a small time. Therefore, the response time for the probe absorption is predicted to be faster than for the yield of steady probability. As expected, in our calculations the response time for dressing excitation is $(1 \sim 10)\mu$s, typically longer than for the probe absorption $(0.1 \sim 1.0)\mu$s, which is quantitatively consistent with the results as represented in Ref. [27].

To briefly summarize, based on a four-level cascaded system, we find that the maximal excitation probability of

TABLE I. Numerical results with respect to Figs. 5(a1), 5(a2) and 5(b1), 5(b2) are quantitatively given under Rydberg decay rates $\gamma/2\pi =$ 60 kHz and 30 kHz, respectively, to represent the relationship among the maximal dressing probabilities $P^{\rm on}_{N,r}$, the response times $\tau_{N,r}$, $\tau_{N,d}$. For a given γ, the same parameter values can be obtained as long as the ratio Ω_{20}/Ω_1 meets the condition of $\Omega_{20}/\Omega_1 = \sqrt{2\gamma/\Gamma}$. Note that another condition $\Omega_1/\Omega_p \gg 1$ is always met here.

Rydberg decay	Key parameters			Atomic number	Response time		Maximal dressing probability
$\gamma(2\pi \times$ kHz)	$\Omega_1(2\pi \times$ MHz)	$\Omega_{20}(2\pi \times$ MHz)	Ω_{20}/Ω_1	N	$\tau_{N,r}(\mu s)$	$\tau_{N,d}(\mu s)$	$P^{on}_{N,r}$
60	100	14	0.14	1	4.5	5.2	0.10
				2	3.4	5.2	0.16
				3	2.7	5.2	0.21
	30	4.2	0.14	1	4.5	5.2	0.10
				2	3.5	5.2	0.16
				3	2.8	5.2	0.21
30	100	10	0.10	1	6.7	10.4	0.16
				2	4.6	10.4	0.24
				3	3.6	10.4	0.29
	30	3	0.10	1	6.8	10.4	0.16
				2	4.7	10.4	0.24
				3	3.7	10.4	0.29

a Rydberg-dressed state is only determined by a relative strength between two strong coupling fields Ω_1 and Ω_{20}, rather than their absolute values under the relationship of $\Omega_1/\Omega_p \gg 1$, offering a great challenge to save the coupling laser powers in a real experimental implementation. However, we also note that although the excitation probability is maximized by Eq. (8) the system may suffer from a longer response time $\tau_{r,d} \sim 200\Gamma^{-1}$, promoting a further study of the effect of blockaded interaction on response times in an ensemble of a few interacting atoms.

IV. SIZABLE RYDBERG-RYDBERG INTERACTIONS

In this section we investigate how the van der Waals(vdWs) interaction affects the transient dressing dynamics in a system of few atoms. To our knowledge, a two-atom system is the simplest model to study the collective feature that has been widely achieved in experiments [41–43]. For that reason we first adopt two atoms with tunable vdWs interactions denoted as $V_{\rm vdW}$, performed by varying the interatomic spacing R. For the interaction strength much larger than Rabi frequencies, the collective Rabi oscillation will be enhanced by a factor of $\sqrt{2}$, leading to an enhancement for the dressing probability [44]; however, it may break due to the invalidity of the full blockaded condition [45] or the resonance by anisotropic interactions [46].

Presently, we employ an approach of the two-atom (A and B) master equation where the Hilbert space is expanded by full 4^2 basis vectors, giving rise to a $4^2 \times 4^2$ density matrix ρ', governed by

$$\frac{d\hat{\rho}'}{dt} = i[\hat{\rho}', \hat{\mathcal{H}}_2] + \hat{\mathcal{L}}_2(\hat{\rho}'), \tag{9}$$

where

$$\hat{\mathcal{H}}_2 = \hat{\mathcal{H}}_1^A + \hat{\mathcal{H}}_1^B + \hat{\mathcal{H}}_2^{af}, \tag{10}$$

with $\hat{\mathcal{H}}_1^{A(B)}$ the single-atom Hamiltonian Eq. (1) and $\hat{\mathcal{H}}_2^{af} = V_{\rm vdW}\hat{\sigma}^A_{2,rr}\hat{\sigma}^B_{2,rr}$ describing the vdWs interaction between two Rydberg atoms. The Lindblad operator becomes

$$\hat{\mathcal{L}}_2(\hat{\rho}) = \sum_{i=A,B} \hat{\mathcal{L}}_1^i(\hat{\rho}), \tag{11}$$

presenting the effect of spontaneous decays.

For comparison, the two important parameters quantifying the switch performance are defined similarly. $P_{2,r}(t)$ describes the time-dependent singly excited dressing probability with $P^{\rm on}_{2,r}$ and $P^{\rm off}_{2,r}[\equiv 0]$ for the stationary values when $\Omega_2(t)$ is switched on or off. Here the definition $P^{\rm on}_{2,r} = P^A_{1,r} + P^B_{1,r} - 2P^{AB}_{2,rr}$ is given, ensuring the excitation detection of one atom. Accordingly, $\tau_{2,r(d)}$ represents the response time of $0 \to P^{\rm on}_{2,r}$ (rise time) and $P^{\rm on}_{2,r} \to 0$ (fall time). Intuitively, $P^{\rm on}_{2,r}$ is predicted to be enhanced by $\sqrt{2}$ with respect to $P^{\rm on}_{1,r}$ by the effect of collective excitation under strong blockaded interaction. In fact, this factor can exceed $\sqrt{2}$ in multilevel systems with comparable Rydberg interactions [47].

In the calculations, to give a more comprehensive understanding, the results based on three interacting atoms (A, B, and C) are simultaneously shown, where the interaction term in Hamiltonian $\hat{\mathcal{H}}_3$ should be replaced by a summation of arbitrary two-atom interactions in the system, given by

$$\hat{\mathcal{H}}_3^{af} = \sum_{\{i>j\}\in(A,B,C)} V_{\rm vdW}\hat{\sigma}^i_{3,rr}\hat{\sigma}^j_{3,rr} \tag{12}$$

as well as the Lindblad operator replaced by $\hat{\mathcal{L}}_3(\hat{\rho}) = \sum_{i=A,B,C}\hat{\mathcal{L}}_1^i(\hat{\rho})$.

Numerical solving Eq. (9) gives rise to an observable measurement for the singly excited-state dressing probability $P_{2,r}(t)$ as well as the response behavior $\tau_{2,r(d)}$. Here we pay attention to the steady dressing probability $P^{\rm on}_{2,r}$ under the switch-on case, and a complete time-dependent output will be considered in Sec. V. In Sec. III we have verified that the maximal dressing probability of single atom under the constraint of Eq. (8) is $P^{\rm on}_{1,r} \approx 0.10$. Turning to the picture of two (three) interacting atoms, due to the collective feature induced by strong interatomic interactions, $P^{\rm on}_{2,r}$ and $P^{\rm on}_{3,r}$ reveal an explicit improvement whose enhancement factor is

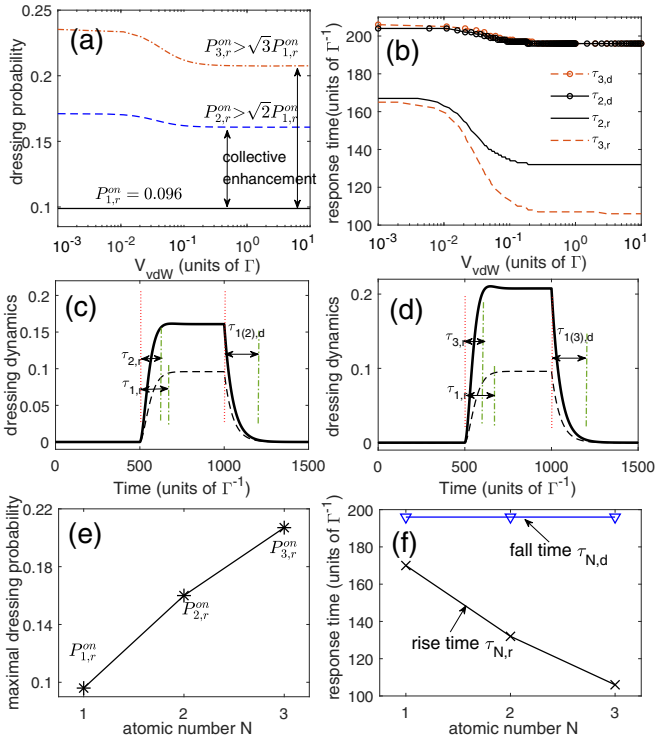

FIG. 4. (a) The singly excited-state dressing probabilities $P^{\rm on}_{3,r}$ (red dash-dotted), $P^{\rm on}_{2,r}$ (blue-dashed) and $P^{\rm on}_{1,r}$ (black-solid) for different atoms $N = 3, 2, 1$, versus the Rydberg interaction strength $V_{\rm vdW}$. (b) The rise time $\tau_{N,r}$(solid and dashed curves) and the fall time $\tau_{N,d}$ (solid and dashed curves with circles) of atom N, versus the interaction $V_{\rm vdW}$. (c) shows the sensitivity of the dressing dynamics with respect to the interaction strength. The one-atom and two-atom results under strong blockaded interaction $V_{\rm vdWs} = 10$ are comparably given by dashed and solid curves. The response times are also labeled. (d) is similar to (c) except for the case between one-atom and three-atom. (e, f) The maximal dressing probability $P^{\rm on}_{N,r}$ and the required response time $\tau_{N,r(d)}$, versus the atomic number N under strong blockaded interaction. Other parameters are $\Omega_p = 0.1$, $\Omega_1 = 5.0$, $\gamma = 0.01$, $\Omega_{20} = \sqrt{2\gamma}\Omega_1 \approx 0.707$, $\Delta_m = 0$, and Γ is the frequency unit.

predicted to be larger than $\sqrt{N}$ (N is the number of atoms) in the strong blockade regimes. Verified by Fig. 4(a) where we present the maximal dressing probability $P^{\rm on}_{N,r}$ as a function of $V_{\rm vdWs}$, and a smoothly decreasing change of $P^{\rm on}_{2(3),r}$ is found while increasing $V_{\rm vdWs}$; in addition $P^{\rm on}_{2,r}$ and $P^{\rm on}_{3,r}$ are observed to be slightly larger than $\sqrt{2}P^{\rm on}_{1,r}$ and $\sqrt{3}P^{\rm on}_{1,r}$ with a sufficient interaction strength. In the weak-interaction limit, $P^{\rm on}_{2(3),r}$ reveals an even bigger value due to its definition that a strong blockaded interaction would reduce the probability of one of N atoms' excitation, making the values smaller. Figure 4(b) shows the corresponding response times $\tau_{2,r(d)}$, $\tau_{3,r(d)}$ by the effect of vdWs interaction strength. Based on the fact that the collective feature will induce a faster-responding dynamic property to the probe absorption, we identify that it also works for the time responses of dressing excitation process. The essence for a faster response to the dressing dynamics can be ascribed to a stronger interaction strength making the Rydberg state out of resonance, allowing the relaxation process mainly affected by a big decay rate from the middle excited states. However, the response time tends to be unchanged when the interaction is sufficiently strong that the excitation of two atoms is completely blockaded.

To reveal the sensitivity of dressing dynamics against the interaction strength in Figs. 4(c) and 4(d) we comparably show the one-period dressing dynamics between one- and two(three)-atom systems. In contrast to the case of one atom it is observed that under strong blockaded interaction, the singly excited probability $P^{\rm on}_{2(3),r}$ (solid) with a few atoms can receive an explicit improvement compared to $P^{\rm on}_{1,r}$ (dashed), accompanied by a quite shorter rise time $\tau_{2(3),r} < \tau_{1,r}$; while the fall time is unchanged. Finally a summary for the maximal steady singly excited dressing probability $P^{\rm on}_{N,r}$ and the corresponding response times are represented in Figs. 4(e) and 4(f), versus the change of atomic number N, proving a robust excitation enhancement with faster rising responses accessible within the scheme of a few atoms. The unchanged fall time $\tau_{N,d}$ is determined by the Rydberg decay γ as discussed later.

V. OPTIMAL EXPERIMENTAL IMPLEMENTATION

A practical dynamic dressed-atom generation via coherent control pulses can be considered using ^{133}Cs atoms with relevant states $|g\rangle = |6S_{1/2}\rangle$, $|m\rangle = |6P_{3/2}$, $|e\rangle = |7S_{1/2}\rangle$, $|r\rangle = |26P_{3/2}\rangle$, carried out by an experimental setup like Fig. 1(c). In the calculations some parameters are estimated to be constant, i.e., $\Gamma/2\pi = 6.0\,$MHz, $\Omega_p/2\pi = 0.6\,$MHz [48]. For two- or three-atom case, we assume a strong blockaded interaction by considering $C_6/2\pi = 140\,{\rm GHz}\mu{\rm m}^6$ and the interatomic spacing $R = 3.64\,\mu$m, giving rise to $V_{\rm vdW}/2\pi = 60\,$MHz [49].

For a comparable representation, in Fig. 5 we study the real dynamic output of atomic dressing probability $P_{N,r}(t)$ to the singly excited Rydberg state by adopting different Rydberg decay rates: $\gamma/2\pi = 60\,$kHz (left panels) and $\gamma/2\pi = 30\,$kHz (right panels). For $\gamma/2\pi = 60\,$kHz ($\gamma/\Gamma = 0.01$) according to the constraints in Eq. (8) the least requirement is

$$\Omega_{20}/\Omega_1 = 0.14, \Omega_1 = 30\,{\rm MHz}, \tag{13}$$

giving rise to a perfect dressing dynamics as shown in Fig. 5(a2), in which the laser Rabi frequencies Ω_{20} and Ω_1 have attained their least but optimal values. Therefore, if Ω_1 exceeds its least-required value but preserving the optimal relationship between Ω_{20} and Ω_1, then the dressed-population dynamics is exactly the same as Fig. 5(a2), taking Fig. 5(a1) as an example. However, once one of these conditions breaks, the probability output will suffer from a significant reduction, as represented in Figs. 5(a3) and 5(a4), which correspond to the breakup of first and second conditions. To this end we stress again the importance of this generalized condition of laser Rabi frequencies in a four-level cascaded system, which not only gives the least laser power of the middle field Ω_1 as compared to the weak probe laser Ω_p, but also determines an optimal relationship between two strong coupling lasers, resulting in a maximal dressing excitation. In other words, the laser powers required in exciting to a highly excited Rydberg state based on a multilevel cascaded system can be strongly saved under the optimal constraint conditions, providing more prospectives for a future experimental implementation.

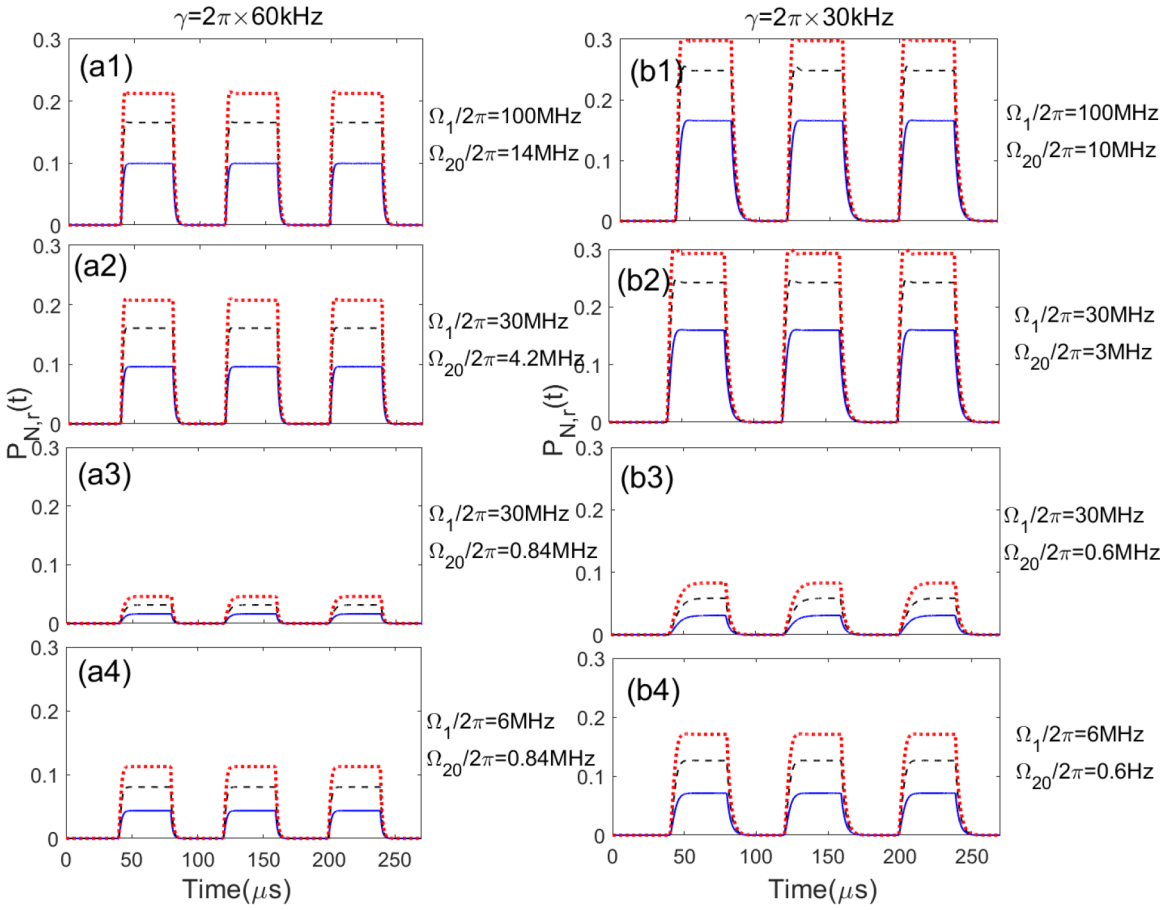

FIG. 5. Realistic performance for time-dependent singly excited dressing probabilities $P_{N,r}$ with different atomic numbers $N = 1$ (blue solid), 2 (black dashed), 3 (red dotted). The required laser Rabi frequencies are denoted on the right of panels and the corresponding Rydberg decay rate is shown on the top. Other parameters are $\Gamma/2\pi = 6.0\,\mathrm{MHz}$, $\Omega_p/2\pi = 0.6\,\mathrm{MHz}$, $\Delta_m = 0$.

Note that the Rydberg decay γ (Γ is the frequency unit) is a key parameter in the consideration that affects the maximal probability as well as the response time. So we repeatedly calculate similar results as Figs. 5(a1)–5(a4) but with a lower decay rate $\gamma/2\pi = 30\,\mathrm{kHz}$. Here the uppermost level is replaced by a higher-n level, e.g., $|r\rangle \approx |nP_{3/2}\rangle$ and $n = 30 \sim 35$ [48]. It is observed that the generalized conditions also works except that the first condition is turn to be $\Omega_{20}/\Omega_1 = \sqrt{2\gamma/\Gamma} \approx 0.1$, giving rise to a higher maximal probability $P_{1,r}^{\mathrm{on}} \approx 0.16$ in contrast to $P_{1,r}^{\mathrm{on}} \approx 0.10$ for $\gamma/2\pi = 60\,\mathrm{kHz}$. The longer response times by lowering the decay rate can be roughly seen in Figs. 5(b1)–5(b4)

Specific parameters including the response times, the maximal dressing probability as well as the required laser Rabi frequencies are summarized in Table I, presenting a quantitative comparison to show the advantage of our scheme. For $\gamma/2\pi = 60\,\mathrm{kHz}$, when $\Omega_1/2\pi = 30\,\mathrm{MHz}$ and $\Omega_{20}/2\pi = 4.2\,\mathrm{MHz}$ are the least but optimal constraint conditions for Rydberg dressing, it is interesting to obtain exactly same values if Ω_1 and Ω_{20} are tuned to be $2\pi \times 100\,\mathrm{MHz}$ and $2\pi \times 14\,\mathrm{MHz}$ where we have relaxed the first constraint but preserved the second one in Eq. (8). Common results are attainable which are $P_{N,r}^{\mathrm{on}} = (0.10, 0.16, 0.21)$, $\tau_{N,r} = (4.5, 3.4, 2.7)\,\mu\mathrm{s}$ and $\tau_{N,d} = 5.2\,\mu\mathrm{s}$ respectively for atoms $N = 1, 2, 3$. Obviously, the increase of atomic number N for strongly interacting atoms allows the rise time to be continuously decreasing from $4.5\,\mu\mathrm{s}$ for $N = 1$ to $2.7\,\mu\mathrm{s}$ for $N = 3$. At the same time the fall time $\tau_{N,d}$ is unvaried. Our results are comparable to the experimental data [$\sim\mu s$] for collective Rabi oscillation and excitation dynamics with Rydberg states [50–52].

By lowering the Rydberg decay γ, except that the constraint condition is preserved we note that the response times $\tau_{N,r}$ and $\tau_{N,d}$ both have a big increase especially for the fall time due to a slower decay rate to the ground states with $P_{N,r}^{\mathrm{off}} = 0$. A slight increase of the rise time can be understood by increasing steady-state population as γ reduces (Fig. 6), requiring more time to reach a higher stationary state.

Finally, it is remarkable that, comparing to the coupling laser Rabi frequencies typically around $\sim$100 MHz for a multilevel cascaded excitation by current experiments [53], we propose an approach that can save this value to be $\sim$10 MHz or smaller, accompanied by an optimal adjustment for the transient response property, robustly facilitating its future use in preparation of higher-n Rydberg atoms with cascaded systems.

VI. CONCLUSIONS

We propose a four-level cascaded scheme for switchable collective dressing excitation using a double Rydberg-EIT

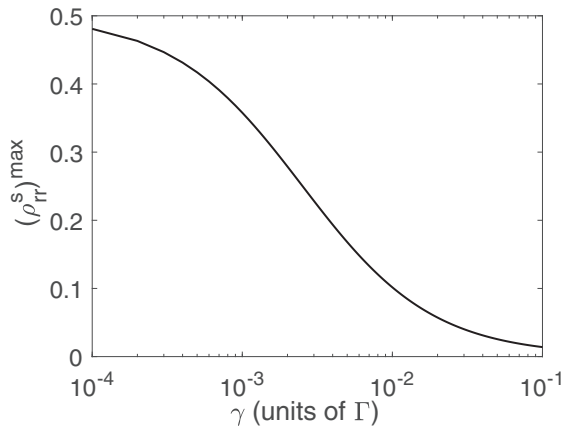

FIG. 6. The maximal stationary dressing probability $(\rho^s_{rr})^{\max}$ versus the decay rate γ. $\Omega_p = 0.1$ and Γ is the frequency unit.

where the control operation is played by the third addressing laser with time-dependent property that directly connects to the Rydberg level. Special attention is payed on the optimization of dressing probability that a generalized condition to a maximal value is attainable which exactly depends on the relative strength of two strong coupling fields. Besides we also explore the transient responses of system by a sudden switch of the pulsed laser, demonstrating the required response time toward a new steady state. While turning to a few atoms with strong interatomic interactions both the dressing probability and the response time are improved due to the collective feature in the blockaded regime.

Remarkably our scheme provides a fresh way to save the laser powers (only depend on the relative strength) in dressing ground atoms to Rydberg levels for a multilevel cascaded system, facilitating a robust and efficient Rydberg-dressed-atom generation with reduced laser powers and optimal response times. An extension to a few-atom ensemble promotes extra advantages in developing a more efficient excitation probability with deeply reduced rise time, widely broadening its applications in controllable many-body physics as well as the quantum control of multilevel drivings.

ACKNOWLEDGMENTS

This work was supported by the National Natural Science Foundation of China under Grants No. 11474094, No. 11104076, by the Science and Technology Commission of Shanghai Municipality under Grant No. 18ZR1412800 and by the Academic Competence Funds for the outstanding doctoral students under Grant No. YBNLTS2019-023.

APPENDIX A: ANALYTICAL STEADY-STATE SOLUTIONS

Here, we present a detailed derivation to calculate the analytical expressions of stationary probe absorption and Rydberg dressing probability in the case of one atom, to quantitatively compare with our numerical calculations. Given the Hamiltonian Eq. (1) and the master Eq. (4), the optical Bloch equations for elements ρ_{ij} of one-atom density $\hat{\rho}$ matrix can be written as

$$\begin{aligned}
\dot{\rho}_{gg} &= \Gamma\rho_{mm} - \Omega_p\rho^I_{gm} + \gamma\rho_{rr},\\
\dot{\rho}_{mm} &= \Gamma(\rho_{ee} - \rho_{mm}) - \Omega_1\rho^I_{me} + \Omega_p\rho^I_{gm},\\
\dot{\rho}_{ee} &= -\Gamma\rho_{ee} + \gamma\rho_{rr} - \Omega_{20}\rho^I_{er} + \Omega_1\rho^I_{me},\\
\dot{\rho}_{rr} &= -2\gamma\rho_{rr} + \Omega_{20}\rho^I_{er},\\
\dot{\rho}_{gm} &= \left(-\frac{\Gamma}{2} - i\Delta_m\right)\rho_{gm} + \frac{i\Omega_p}{2}(\rho_{gg} - \rho_{mm}) + \frac{i\Omega_1}{2}\rho_{ge},\\
\dot{\rho}_{ge} &= \left(-\frac{\Gamma}{2} - i\Delta_m\right)\rho_{ge} + \frac{i\Omega_1}{2}\rho_{gm} + \frac{i\Omega_{20}}{2}\rho_{gr} - \frac{i\Omega_p}{2}\rho_{me},\\
\dot{\rho}_{gr} &= (-\gamma - i\Delta_m)\rho_{gr} + \frac{i\Omega_{20}}{2}\rho_{ge} - \frac{i\Omega_p}{2}\rho_{mr},\\
\dot{\rho}_{me} &= -\Gamma\rho_{me} + \frac{i\Omega_1}{2}(\rho_{mm} - \rho_{ee}) + \frac{i\Omega_{20}}{2}\rho_{mr} - \frac{i\Omega_p}{2}\rho_{ge},\\
\dot{\rho}_{mr} &= \left(-\frac{\Gamma + 2\gamma}{2}\right)\rho_{mr} - \frac{i\Omega_1}{2}\rho_{er} + \frac{i\Omega_{20}}{2}\rho_{me} - \frac{i\Omega_p}{2}\rho_{gr},\\
\dot{\rho}_{er} &= \left(-\frac{\Gamma + 2\gamma}{2}\right)\rho_{er} - \frac{i\Omega_1}{2}\rho_{mr} + \frac{i\Omega_{20}}{2}(\rho_{ee} - \rho_{rr}),
\end{aligned} \tag{A1}$$

where the population $\rho_{gg} + \rho_{mm} + \rho_{ee} + \rho_{rr} = 1$ is conserved. With the steady-state assumption $\dot{\rho}_{ij} = 0$ all steady state solutions ρ^s_{ij} (superscript s means the stationary solution) are analytically solvable from Eq. (A1), part of which are presented here.

We start with the weak-probe limit that $\rho^s_{gg} = 1$ and $\rho^s_{jj} = 0$, $j \in \{m, e, r\}$ is assumed. Inserting $\rho^s_{gg} = 1$ and ρ^s_{jj} into the nondiagonal element equations of Eqs. (A1), ρ^s_{gm} can be derived taking the form of

$$\rho^s_{gm} = i\Omega_p\frac{\Omega^2_{20} + X_1X_2}{X_1\Omega^2_{20} + X_2\Omega^2_1 + X^2_1X_2}, \tag{A2}$$

with $X_1 = \Gamma + 2i\Delta_m$, $X_2 = 2\gamma + 2i\Delta_m$ and $\Gamma_m = \Gamma_e = \Gamma, \Gamma_r = \gamma$. The imaginary part of ρ^s_{gm} to the first-order perturbation under $\Omega_1, \Omega_{20} \gg \Omega_p$, presenting the stationary probe absorption, is described by

$$\frac{(\rho^I_{gm})^s}{\Omega_p} = \frac{4\gamma^2(1+\Omega^2_1) + 2\gamma(2+\Omega^2_1)\Omega^2_{20} + \left[4\Delta^2_m + 16\Delta^4_m + \Omega^4_{20} + 4\Delta^2_m(\Omega^2_1 - 2\Omega^2_{20})\right]}{4\Delta^2_m + 4\gamma^2(1+\Omega^2_1)^2 + 4\gamma(1+\Omega^2_1)\Omega^2_{20} + 4\Delta^2_m(\Omega^2_1 + \Omega^2_{20} - 4\Delta^2_m)^2 + 32\Delta^4_m + \Omega^4_{20} + 8\Delta^2_m(\Omega^2_1 - \Omega^2_{20})}. \tag{A3}$$

It is worth noting that $(\rho^I_{gm})^s \propto \Omega_p$, arising the probe absorption strength linearly increased with the probe laser intensity.

Next, by substituting ρ^s_{gm} and other nondiagonal stationary elements (not shown) into the steady-state equations $\dot{\rho}_{ij} = 0$ we arrive at a more complex expression describing the steady dressing probabilities of Rydberg state, which is given by

$$\rho^s_{rr} = \frac{\Omega_1^2\Omega_{20}^2\left(2+\Omega_1^2+\Omega_{20}^2\right)\Omega_p^2}{4\gamma^2\left(\Omega_1^2+1\right)^3+\Omega_{20}^4\left(2+\Omega_1^2+\Omega_{20}^2\right)+\Omega_{20}^2\left[2+5\Omega_1^2+2\left(\Omega_1^4+\Omega_{20}^4\right)\right]\Omega_p^2+2\gamma\left[2\Omega_{20}^2\left(2+\Omega_1^4+3\Omega_1^2+2\Omega_{20}^2\right)+\left(2+\Omega_1^2\right)^2\Omega_p^2\right]}, \tag{A4}$$

according to $\Delta_m = 0$, and

$$\rho^s_{rr} = \frac{\Omega_1^2\Omega_{20}^2\Omega_p^2\left[4\gamma+6\gamma\Omega_1^2+2\Omega_1^4+\left(2+3\Omega_1^2\right)\Omega_{20}^2+\Omega_{20}^4\right]}{\left[2\gamma\left(1+\Omega_1^2\right)\left(2+\Omega_1^2\right)+\Omega_{20}^2\left(2+\Omega_1^2+\Omega_{20}^2\right)\right]\left[\left(\Omega_1^2+\Omega_{20}^2\right)+\left(2\Omega_1^2+\Omega_{20}^2\right)^2\right]}, \tag{A5}$$

according to $\Delta_m = \pm\Omega_{\rm eff}/2$. Notice that all physical quantities in Eqs. (A3)–(A5) have been scaled by the frequency unit Γ. Due to the complexity, Eqs. (A3)–(A5) are plotted in Figs. 2(c) and 2(d) by circles, as compared with our full numerical results (solid curves) solved from optical Bloch Eq. (A1) directly. A perfect agreement is revealed [see Figs. 2(c) and 2(d)], strongly supporting the correctness of our calculations.

By doing a derivation to Eq. (A4) with respect to the ratio of Ω_{20}/Ω_1 it arrives at an approximated relationship

$$\frac{\Omega_{20}}{\Omega_1} \approx \sqrt{2\gamma/\Gamma}, \tag{A6}$$

by which a maximal steady dressing probability $(\rho^s_{rr})^{\max}$ under the constraint of $\Omega_1 \gg \Omega_p$, can be expressed as

$$(\rho^s_{rr})^{\max} = \frac{(1+2\gamma)\Omega_p^2}{2\Omega_p^2+4\gamma(2+\gamma)}. \tag{A7}$$

Figure 6 represents that $(\rho^s_{rr})^{\max}$ continuously decreases as γ increases. In the calculation we choose $\gamma = 0.01$, $\Omega_p = 0.1$ and Γ is the frequency unit, arising the maximal probability $(\rho^s_{rr})^{\max} \approx 0.1016$ at $\Omega_{20}/\Omega_1 = 0.1414$.

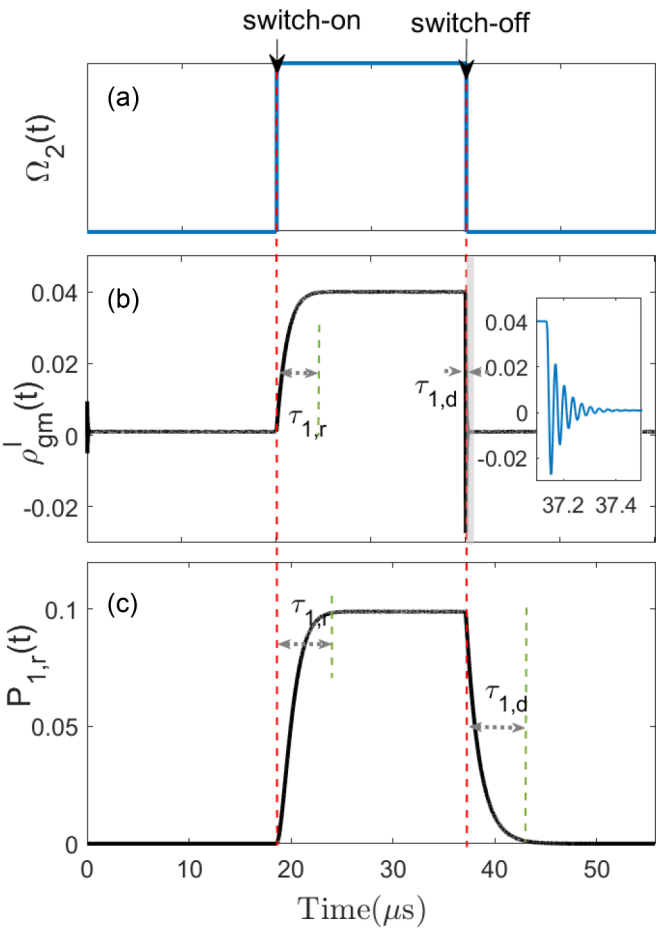

FIG. 7. A comparison of transient response times between the probe absorption and dynamic dressing processes. (a) The one-period square-wave pulse sequence $\Omega_2(t)$; (b, c) show a practical time dependence of the probe absorption $\rho^I_{gm}(t)$ and the Rydberg dressing probability $P_{1,r}(t)$ where the rise time $\tau_{1,r}$ and fall time $\tau_{1,d}$ are both represented. Inset of (b) is an enlarged picture for showing the fast damped oscillations to the fall-time response of probe absorption when the addressing laser is suddenly switched off. Parameters are the same as used in Fig. 5(a2).

APPENDIX B: COMPARING RESPONSE TIMES OF PROBE ABSORPTION AND DYNAMIC DRESSING

In this Appendix, we numerically compare different transient responses for the probe absorption $\rho^I_{gm}(t)$ (as studied by Zhang in Ref. [27]) and the Rydberg dressing probability $P_{1,r}(t)$ by doing a sudden switch of $\Omega_2(t)$, proving that the required response time for the dressing is longer than for the probe absorption, especially the fall time $\tau_{1,d}$. A numerical search algorithm is carried out by tracking the minimal time required towards a new steady state through a sudden switch of the addressing pulse.

Figure 7(a) shows the shape of an one-period control pulse $\Omega_2(t)$ where the operations of switch-on or switch-off occur at $t = 18.57\,\mu$s and $37.14\,\mu$s, respectively. With the incidence of such a pulse we numerically calculate the realistic dynamics of $\rho^I_{gm}(t)$ and $P_{1,r}(t)$ as displayed in Figs. 7(b) and 7(c), where the rise and fall times are importantly denoted. In general, it is observed that both $\rho^I_{gm}(t)$ and $P_{1,r}(t)$ represent an in-phase

TABLE II. By switching on or off the addressing laser $\Omega_2(t)$ a quantitative comparison for the transient response times of $\rho^I_{gm}(t)$ and $P_{1,r}(t)$ are given, corresponding to the results in Figs. 7(b) and 7(c).

Measured variables	$\tau_{1,r}(\mu s)$	$\tau_{1,d}(\mu s)$
$\rho^I_{gm}(t)$	3.326	0.202
$P_{1,r}(t)$	4.475	5.194

behavior toward its new steady states with respect to $\Omega_2(t)$, however, accompanied by quite different response times. A quantitative comparison of response times is given in Table II showing that the rise and fall times of $P_{1,r}(t)$ is relatively longer, caused by a small decay rate of highly excited Rydberg state.

In addition it is notable that the fall time $\tau_{1,d}$ of $\rho^I_{gm}(t)$ is significantly shorter than of $P_{1,r}(t)$ by more than one order of magnitude, accordingly in the inset of Fig. 7(b) the behavior $\rho^I_{gm}(t)$ has an ultrafast damped oscillation to be stable. The reason for that can be understood by the relaxation process in a driven-dissipative system, quantitatively coinciding with the timescale as found in Ref. [27]. Therefore we conclude that a practical operation on preparing Rydberg-dressed atoms requires a timescale of $(1 \sim 10)\,\mu$s, longer than the time for recording the transient response of probe laser transmission in the EIT environment, which typically needs $(0.1 \sim 1.0)\,\mu$s by experimentalists [54].

[1] J. E. Johnson and S. L. Rolston, Interactions between Rydberg-dressed atoms, Phys. Rev. A **82**, 033412 (2010).

[2] M. Saffman, Quantum computing with atomic qubits and Rydberg interactions: Progress and challenges, J. Phys. B **49**, 202001 (2016).

[3] J. Honer, H. Weimer, T. Pfau, and H. P. Büchler, Collective Many-Body Interaction in Rydberg-Dressed Atoms, Phys. Rev. Lett. **105**, 160404 (2010).

[4] G. Pupillo, A. Micheli, M. Boninsegni, I. Lesanovsky, and P. Zoller, Strongly Correlated Gases of Rydberg-Dressed Atoms: Quantum and Classical Dynamics, Phys. Rev. Lett. **104**, 223002 (2010).

[5] N. Henkel, R. Nath, and T. Pohl, Three-Dimensional Roton Excitations and Supersolid Formation in Rydberg-Excited Bose-Einstein Condensates, Phys. Rev. Lett. **104**, 195302 (2010).

[6] J. Balewski, A. Krupp, A. Gaj, S. Hofferberth, R. Löw, and T. Pfau, Rydberg dressing: Understanding of collective many-body effects and implications for experiments, New J. Phys. **16**, 063012 (2014).

[7] R. M. W. van Bijnen and T. Pohl, Quantum Magnetism and Topological Ordering via Rydberg Dressing Near Förster Resonances, Phys. Rev. Lett. **114**, 243002 (2015).

[8] A. W. Glaetzle, M. Dalmonte, R. Nath, C. Gross, I. Bloch, and P. Zoller, Designing Frustrated Quantum Magnets with Laser-Dressed Rydberg Atoms, Phys. Rev. Lett. **114**, 173002 (2015).

[9] T. Keating, K. Goyal, Y.-Y. Jau, G. W. Biedermann, A. J. Landahl, and I. H. Deutsch, Adiabatic quantum computation with Rydberg-dressed atoms, Phys. Rev. A **87**, 052314 (2013).

[10] T. Keating, R. L. Cook, A. M. Hankin, Y.-Y. Jau, G. W. Biedermann, and I. H. Deutsch, Robust quantum logic in neutral atoms via adiabatic Rydberg dressing, Phys. Rev. A **91**, 012337 (2015).

[11] Y. Jau, A. Hankin, T. Keating, I. Deutsch, and G. Biedermann, Entangling atomic spins with a Rydberg-dressed spin-flip blockade, Nat. Phys. **12**, 71 (2016).

[12] A. K. Mohapatra, T. R. Jackson, and C. S. Adams, Coherent Optical Detection of Highly Excited Rydberg States Using Electromagnetically Induced Transparency, Phys. Rev. Lett. **98**, 113003 (2007).

[13] J. D. Pritchard, D. Maxwell, A. Gauguet, K. J. Weatherill, M. P. A. Jones, and C. S. Adams, Cooperative Atom-Light Interaction in a Blockaded Rydberg Ensemble, Phys. Rev. Lett. **105**, 193603 (2010).

[14] D. Petrosyan, J. Otterbach, and M. Fleischhauer, Electromagnetically Induced Transparency with Rydberg Atoms, Phys. Rev. Lett. **107**, 213601 (2011).

[15] C. Gaul, B. J. DeSalvo, J. A. Aman, F. B. Dunning, T. C. Killian, and T. Pohl, Resonant Rydberg Dressing of Alkaline-Earth Atoms via Electromagnetically Induced Transparency, Phys. Rev. Lett. **116**, 243001 (2016).

[16] O. Firstenberg, C. Adams, and S. Hofferberth, Nonlinear quantum optics mediated by Rydberg interactions, J. Phys. B **49**, 152003 (2016).

[17] T. Vogt, C. Gross, T. Gallagher, and W. Li, Microwave-assisted Rydberg electromagnetically induced transparency, Opt. Lett. **43**, 1822 (2018).

[18] S. deLeseleuc, D. Barredo, V. Lienhard, A. Browaeys, and T. Lahaye, Optical Control of the Resonant Dipole-Dipole Interaction between Rydberg Atoms, Phys. Rev. Lett. **119**, 053202 (2017).

[19] C. Carr, M. Tanasittikosol, A. Sargsyan, D. Sarkisyan, C. Adams, and K. Weatherill, Three-photon electromagnetically induced transparency using Rydberg states, Opt. Lett. **37**, 3858 (2012).

[20] G. S. Agarwal and W. Harshawardhan, Inhibition and Enhancement of Two Photon Absorption, Phys. Rev. Lett. **77**, 1039 (1996).

[21] S. E. Harris and Y. Yamamoto, Photon Switching by Quantum Interference, Phys. Rev. Lett. **81**, 3611 (1998).

[22] N. Mulchan, D. Ducreay, R. Pina, M. Yan, and Y. Zhu, Nonlinear excitation by quantum interference in a Doppler-broadened rubidium atomic system, J. Opt. Am. B **17**, 820 (2000).

[23] B. Dutta and P. Mahapatra, Nonlinear optical effects in a doubly driven four-level atom, Phys. Scr. **75**, 345 (2007).

[24] J. Che, H. Zheng, Z. Zhang, X. Yao, C. Li, Z. Wu, and Y. Zhang, Rydberg dressing evolution via Rabi frequency control in thermal atomic vapors, Phys. Chem. Chem. Phys. **16**, 18840 (2014).

[25] J. Kondo, N. Sibalic, A. Guttridge, C. Wade, N. Melo, C. Adams, and K. Weatherill, Observation of interference effects via four-photon excitation of highly excited Rydberg states in thermal cesium vapor, Opt. Lett. **40**, 5570 (2015).

[26] C. Veit, G. Epple, H. Kübler, T. Euser, P. Russell, and R. Löw, RF-dressed Rydberg atoms in hollow-core fibres, J. Phys. B **49**, 134005 (2016).

[27] Q. Zhang, Z. Bai, and G. Huang, Fast-responding property of electromagnetically induced transparency in Rydberg atoms, Phys. Rev. A **97**, 043821 (2018).

[28] C. Ates, S. Sevinçli, and T. Pohl, Electromagnetically induced transparency in strongly interacting Rydberg gases, Phys. Rev. A **83**, 041802(R) (2011).

[29] W. Xu and B. De Marco, Velocity-selective electromagnetically induced-transparency measurements of potassium Rydberg states, Phys. Rev. A **93**, 011801(R) (2016).

[30] J. Sheng, Y. Chao, S. Kumar, H. Fan, J. Sedlacek, and J. P. Shaffer, Intracavity Rydberg-atom electromagnetically induced

transparency using a high-finesse optical cavity, Phys. Rev. A **96**, 033813 (2017).

[31] Y. Jiao, L. Hao, X. Han, S. Bai, G. Raithel, J. Zhao, and S. Jia, Atom-based radio-frequency field calibration and polarization measurement using cesium nD_J Floquet states, Phys. Rev. Appl. **8**, 014028 (2017).

[32] H. Rawat, S. Dubey, and V. Ojha, Distinction between double electromagnetically induced transparency and double Autler-Townes splitting in RF-driven four-level ladder ^{87}Rb atomic vapor, J. Phys. B **51**, 155401 (2018).

[33] X. Chai, L. Zhang, D. Ma, L. Yan, H. Bao, and J. Qian, Anomalous excitation enhancement with Rydberg-dressed atoms, Phys. Rev. A **96**, 053417 (2017).

[34] S. Baur, D. Tiarks, G. Rempe, and S. Dürr, Single-Photon Switch Based on Rydberg Blockade, Phys. Rev. Lett. **112**, 073901 (2014).

[35] H. Gorniaczyk, C. Tresp, J. Schmidt, H. Fedder, and S. Hofferberth, Single-Photon Transistor Mediated by Interstate Rydberg Interactions, Phys. Rev. Lett. **113**, 053601 (2014).

[36] W. Li and I. Lesanovsky, Coherence in a cold-atom photon switch, Phys. Rev. A **92**, 043828 (2015).

[37] J. Qian, Robust quantum switch with Rydberg excitations, Sci. Reps. **7**, 12952 (2017).

[38] D. McGloin, D. Fulton, and M. Dunn, Electromagnetically induced transparency in N-level cascade schemes, Opt. Commun. **190**, 221 (2001).

[39] M. D. Lukin, S. F. Yelin, M. Fleischhauer, and M. O. Scully, Quantum interference effects induced by interacting dark resonance, Phys. Rev. A **60**, 3225 (1999).

[40] L. Zhang, Z. Feng, A. Li, J. Zhao, C. Li, and S. Jia, Measurement of quantum defects of nS and nD states using field ionization spectroscopy in ultracold cesium atoms, Chin. Phys. B **18**, 1838 (2009).

[41] E. Urban, T. Johnson, T. Henage, L. Isenhower, D. Yavuz, T. Walker, and M. Saffman, Observation of Rydberg blockade between two atoms, Nat. Phys. **5**, 110 (2009).

[42] A. Gaëtan, Y. Miroshnychenko, T. Wilk, A. Chotia, M. Viteau, D. Comparat, P. Pillet, A. Browaeys, and P. Grangier, Observation of collective excitation of two individual atoms in the Rydberg blockade regime, Nat. Phys. **5**, 115 (2009).

[43] T. Wilk, A. Gaëtan, C. Evellin, J. Wolters, Y. Miroshnychenko, P. Grangier, and A. Browaeys, Entanglement of Two Individual Neutral Atoms Using Rydberg Blockade, Phys. Rev. Lett. **104**, 010502 (2010).

[44] R. Heidemann, U. Raitzsch, V. Bendkowsky, B. Butscher, R. Löw, L. Santos, and T. Pfau, Evidence for Coherent Collective Rydberg Excitation in the Strong Blockade Regime, Phys. Rev. Lett. **99**, 163601 (2007).

[45] L. Béguin, A. Vernier, R. Chicireanu, T. Lahaye, and A. Browaeys, Direct Measurement of the van der Waals Interaction between Two Rydberg Atoms, Phys. Rev. Lett. **110**, 263201 (2013).

[46] J. Qian, Resonance-enhanced collective effect in a triangle arrangement of Rydberg atoms with anisotropic interactions, J. Opt. Soc. Am. B **33**, 1749 (2016).

[47] D. Ma, K. Zhang, and J. Qian, Properties of collective Rabi oscillations with two Rydberg atoms, Chin. Phys. B **28**, 013202 (2019).

[48] I. I. Beterov, I. I. Ryabtsev, D. B. Tretyakov, and V. M. Entin, Quasiclassical calculations of blackbody-radiation-induced depopulation rates and effective lifetimes of Rydberg nS, nP, and nD alkali-metal atoms with $n \leqslant 80$, Phys. Rev. A **79**, 052504 (2009).

[49] H. Zoubi, Van der Waals interactions among alkali Rydberg atoms with excitonic states, J. Phys. B **48**, 185002 (2015).

[50] T. A. Johnson, E. Urban, T. Henage, L. Isenhower, D. D. Yavuz, T. G. Walker, and M. Saffman, Rabi Oscillations between Ground and Rydberg States with Dipole-Dipole Atomic Interactions, Phys. Rev. Lett. **100**, 113003 (2008).

[51] Y. O. Dudin and A. Kuzmich, Strongly interacting Rydberg excitations of a cold atomic gas, Science **336**, 887 (2012).

[52] J. Zeiher, P. Schauß, S. Hild, T. Macrì, I. Bloch, and C. Gross, Microscopic Characterization of Scalable Coherent Rydberg Superatoms, Phys. Rev. X **5**, 031015 (2015).

[53] N. Šibalić, J. M. Kondo, C. S. Adams, and K. J. Weatherill, Dressed-state electromagnetically induced transparency for light storage in uniform-phase spin waves, Phys. Rev. A **94**, 033840 (2016).

[54] G. Dmochowski, A. Feizpour, M. Hallaji, C. Zhuang, A. Hayat, and A. M. Steinberg, Experimental Demonstration of the Effectiveness of Electromagnetically Induced Transparency for Enhancing Cross-Phase Modulation in the Short-Pulse Regime, Phys. Rev. Lett. **116**, 173002 (2016).